

Bayesian Physics-Informed Neural Networks for Inverse Problems (BPINN-IP): Application in Infrared Image Processing

Ali Mohammad-Djafari^{a,*}, Ning Chu^b, Li Wang^c

^a*former CNRS, founder of ISCT, Bures-sur-Yvette, France
Researcher at Shanfeng, Shaoxing and IDT, Ningbo, China
Email: djafari@ieee.org, ORCID: 0000-0003-0678-7759*

^b*IDT, Ningbo, China
Email: chuning1983@sina.com*

^c*Central South University (CSU), Changsha, China
Email: wang.li@csu.edu.cn*

Abstract

Inverse problems arise across scientific and engineering domains, where the goal is to infer hidden parameters or physical fields from indirect and noisy observations. Classical approaches, such as variational regularization and Bayesian inference, provide well-established theoretical foundations for handling ill-posedness. However, these methods often become computationally restrictive in high-dimensional settings or when the forward model is governed by complex physics.

Physics-Informed Neural Networks (PINNs) have recently emerged as a promising framework for solving inverse problems by embedding physical laws directly into the training process of neural networks. In this paper, we introduce a new perspective on the Bayesian Physics-Informed Neural Network (BPINN) framework, extending classical PINNs by explicitly incorporating training data generation, modeling and measurement uncertainties through Bayesian prior modeling and doing inference with the posterior laws. Also, as we focus on the inverse problems, we

*Corresponding author.

Email address: djafari@ieee.org (Ali Mohammad-Djafari)

call this method BPINN-IP, and we show that the standard PINN formulation naturally appears as its special case corresponding to the Maximum A Posteriori (MAP) estimate.

This unified formulation allows simultaneous exploitation of physical constraints, prior knowledge, and data-driven inference, while enabling uncertainty quantification through posterior distributions. To demonstrate the effectiveness of the proposed framework, we consider inverse problems arising in infrared image processing, including deconvolution and super-resolution, and present results on both simulated and real industrial data.

Keywords: Inverse problems, Physics-informed neural networks (PINN), Bayesian PINN (BPINN), Uncertainty quantification (UQ), Infrared imaging.

1. Introduction

Inverse problems are fundamental in many areas of science and engineering, where the objective is to infer hidden physical quantities from indirect, noisy, or incomplete observations [1, 2, 3, 4]. Applications include medical and biological imaging [5, 6], geophysical exploration [7, 8], and industrial nondestructive evaluation [4].

Traditional approaches to inverse problems rely on analytical formulations, variational regularization, and Bayesian inference [9, 10, 11]. Bayesian inference is particularly appealing because it explicitly accounts for uncertainties by modeling the posterior distribution of the unknowns conditioned on observations [12, 11]. However, classical Bayesian methods such as Markov Chain Monte Carlo (MCMC) or Hamiltonian Monte Carlo can become computationally prohibitive in high-dimensional contexts or when the forward operator is governed by complex physics.

Deep learning (DL) and neural networks (NNs) have recently opened new directions for solving inverse problems [13, 14]. Data-driven architectures can approximate linear or nonlinear mappings between observations and unknowns, but they typically require large labeled datasets and often lack interpretability. Physics-Informed Neural Networks (PINNs) address these limitations by embedding the governing physical laws as soft constraints in the loss function, enabling improved generalization and reduced training data requirements [13, 15].

This paper advances the PINN paradigm by introducing a new Bayesian formulation specifically for inverse problems, referred to as a Bayesian Physics-Informed Neural Network (BPINN-IP). Although the term BPINN has appeared previously [14], our formulation differs in explicitly formulating the uncertainties in the training data generation or their acquisition, as well as prior modeling, which result to obtaining a posterior law for the output of the NN, from which, we can infer on it. In the proposed methodology, we begin by describing a probabilistic generative model that characterizes both the training data and the observation model. We then impose the physical forward operator as a constraint within the Bayesian inference framework, resulting in posterior distributions over the unknown physical fields as well as the neural network parameters.

This formulation unifies deterministic PINNs and Bayesian inference: the classical PINN loss arises as the Maximum A Posteriori (MAP) estimator of the BPINN-IP, while the full BPINN-IP enables both estimates and uncertainty quantification (UQ). The remainder of this paper details the proposed probabilistic formulation, demonstrates its performance through synthetic and real-world infrared imaging examples, and discusses implications for broader classes of inverse problems.

2. Literature Review and State of the Art in NN, PINN, and BPINN Methods for Inverse Problems

Inverse problems have been studied extensively using analytical, variational, and probabilistic approaches. Analytical methods provide exact solutions but are limited to simple, well-posed configurations [9]. Variational regularization techniques—such as Tikhonov regularization [10] and sparsity-promoting priors—are widely used to stabilize ill-posed character of inverse problems [16], though selecting appropriate regularization parameters remains challenging, especially in noisy or heterogeneous environments.

Bayesian inference offers a principled framework for incorporating prior knowledge and quantifying uncertainties [11]. Sampling-based strategies, such as Markov Chain Monte Carlo (MCMC) [17] and Hamiltonian Monte Carlo [18], allow exploration of complex posterior distributions but often suffer from high computational cost. Variational approximate inference methods provide more scalable approximations, yet may struggle to capture multimodal or high-dimensional posterior geometries.

Deep learning has significantly advanced inverse problem-solving capabilities via its capability of doing fast inference. Convolutional (CNN) and recurrent neural networks (RNN) learn complex nonlinear mappings from data [5, 8], but their dependence on large labeled datasets and limited interpretability can hinder physical consistency. Physics-Informed Neural Networks (PINNs) address these challenges by incorporating governing equations as soft constraints in the optimization problem, improving generalization and reducing data requirements [13].

Recent developments have extended PINNs to Bayesian formulations (often termed BPINNs), introducing stochastic regularization, probabilistic priors, or approximate posterior inference [14]. While these approaches are promising, significant gaps remain in terms of training robustness, integration of forward-model uncertainties, and validation on real-world experimental datasets.

In this work, we build on these foundations by proposing a new Bayesian PINN framework specifically tailored for inverse problems, that we call (BPINN-IP). The method begins with a generative prior model describing the training data, proceeds with a Bayesian interpretation of the training process, and incorporates the forward physical model to derive posterior laws for both the unknown physical quantities and the neural network parameters. We show explicitly that deterministic PINNs arise as a special case corresponding to the MAP solution of the BPINN-IP. The resulting framework combines the interpretability and physical consistency of PINNs with the principled uncertainty quantification of Bayesian inference, yielding a robust and general methodology applicable to both simulated and experimental scenarios.

3. Proposed Bayesian PINN-IP framework

We start by introducing the proposed Bayesian Physics-Informed Neural Network for inverse problems (BPINN-IP) framework in a sequence of five conceptual steps.

1. Forward (generative) model.

We start by assuming a general forward or generative model

$$g = H(f) + \epsilon, \quad (1)$$

where \mathbf{f} is the input (unknown), \mathbf{g} the output (observed data), \mathbf{H} the forward model, and ϵ the (additive) modeling and measurement errors. In the linear case, this simplifies to

$$\mathbf{g} = \mathbf{H}\mathbf{f} + \epsilon, \quad (2)$$

where \mathbf{H} is now a matrix. In many imaging inverse problems, $\mathbf{f} \in \mathbb{R}^N$ is a vector containing all pixels of the unknown image, and $\mathbf{g} \in \mathbb{R}^M$ collects all measured data (which may itself be an image). Thus, $\mathbf{H} \in \mathbb{R}^{M \times N}$.

In realistic imaging problems, M and N can be very large (e.g. for images of size $m \times n$, we have $M = N = m \times n$), making it infeasible to store the whole matrix \mathbf{H} explicitly. Fortunately, practical algorithms only need the forward operator $\mathbf{f} \mapsto \mathbf{H}\mathbf{f}$ and its adjoint $\mathbf{g} \mapsto \mathbf{H}^T \mathbf{g}$, which can often be implemented efficiently without forming explicitly \mathbf{H} explicitly.

2. Prior modeling and Bayesian formulation.

We now assign priors $p(\mathbf{f})$ and $p(\epsilon)$. From the latter and the forward model, we obtain the likelihood $p(\mathbf{g}|\mathbf{f})$. Bayes' rule then gives the posterior

$$p(\mathbf{f}|\mathbf{g}) = \frac{p(\mathbf{g}|\mathbf{f}) p(\mathbf{f})}{p(\mathbf{g})}, \quad (3)$$

where $p(\mathbf{g}|\mathbf{f}) = p(\epsilon)$ with $\epsilon = \mathbf{g} - \mathbf{H}\mathbf{f}$, and

$$p(\mathbf{g}) = \int p(\mathbf{g}|\mathbf{f}) p(\mathbf{f}) d\mathbf{f}.$$

For the class of linear inverse problems $\mathbf{g} = \mathbf{H}\mathbf{f} + \epsilon$ with Gaussian likelihood

$$p(\mathbf{g}|\mathbf{f}) = \mathcal{N}(\mathbf{g} \mid \mathbf{H}\mathbf{f}, v_\epsilon \mathbf{I}),$$

and Gaussian prior

$$p(\mathbf{f}) = \mathcal{N}(\mathbf{f} \mid \bar{\mathbf{f}}, v_f \mathbf{I}),$$

it is well known (and easy to show) that the posterior $p(\mathbf{f}|\mathbf{g})$ is also Gaussian:

$$p(\mathbf{f}|\mathbf{g}) = \mathcal{N}(\mathbf{f} \mid \hat{\mathbf{f}}, \hat{\Sigma}) \quad (4)$$

with

$$\begin{cases} \hat{f} = [\mathbf{H}^T \mathbf{H} + \lambda \mathbf{I}]^{-1} (\mathbf{H}^T \mathbf{g} + \lambda \bar{f}), \\ \hat{\Sigma} = v_\epsilon [\mathbf{H}^T \mathbf{H} + \lambda \mathbf{I}]^{-1}, \quad \lambda = \frac{v_\epsilon}{v_f}. \end{cases} \quad (5)$$

The mean \hat{f} corresponds to the classical Tikhonov solution, and $\hat{\Sigma}$ quantifies its uncertainty.

3. Neural network surrogate for the inverse map.

Next, we design an appropriate neural network that takes \mathbf{g} as input and outputs an estimate f_{NN} of f . This NN can be viewed as an approximate inverse or surrogate:

$$\mathbf{g} \Rightarrow \boxed{\text{NN}(\mathbf{w})} \Rightarrow f_{NN},$$

where \mathbf{w} denotes the NN parameters. The crucial task is to choose an appropriate network architecture: input layer, number and sizes of hidden layers, output layer, connections, activation functions, and thus the dimension of the parameter vector \mathbf{w} . In many imaging applications, U-Net-like architectures are particularly convenient, but the proposed framework is agnostic to the specific choice.

4. Training the NN: supervised and unsupervised cases.

We distinguish two main training scenarios.

- **Supervised case.** Here, we have a set of training pairs $\{\mathbf{g}_{Ti}, \mathbf{f}_{Ti}\}$, where \mathbf{f}_{Ti} are reference (ground-truth) images. The training step estimates the NN parameters $\hat{\mathbf{w}}$, schematically:

$$\begin{array}{c} \text{Data} \\ \{\mathbf{g}_{Ti}, \mathbf{f}_{Ti}\} \end{array} \Rightarrow \boxed{\begin{array}{c} \text{Training step} \\ \text{NN}(\mathbf{w}) \end{array}} \Rightarrow \hat{\mathbf{w}}.$$

- **Unsupervised case.** Here, only the degraded data $\{\mathbf{g}_{Ti}\}$ are available. Classical NNs cannot handle this situation directly, whereas the PINN approach, thanks to the physics-informed part of the loss, can still be trained and yield an estimate $\hat{\mathbf{w}}$:

$$\begin{array}{c} \text{Data} \\ \{\mathbf{g}_{Ti}\} \end{array} \Rightarrow \boxed{\begin{array}{c} \text{Training step} \\ \text{NN}(\mathbf{w}) \end{array}} \Rightarrow \hat{\mathbf{w}}.$$

The index i enumerates the samples in the training dataset. At the end of training, we obtain an estimate \hat{w} of the NN parameters. The training step is generally the most computationally demanding phase and requires careful choice of the optimization criterion and algorithm.

In standard supervised regression, the loss is the classical output-error loss

$$J_{NN}(w) = \sum_i \|f_{NNi}(w) - f_{Ti}\|^2,$$

where $f_{NNi}(w)$ is the NN output for input g_{Ti} , and f_{Ti} is the corresponding ground truth. Later, additional terms will be added to this loss, either for regularization or to enforce physics-informed constraints.

After defining the loss, we choose an optimization algorithm, typically gradient-based (stochastic gradient descent and its variants), along with hyperparameters such as learning rate, number of iterations, and stopping criteria. Hyperparameter tuning is often necessary to obtain good generalization and to avoid overfitting.

5. **Inference and uncertainty quantification.** Once the NN has been trained, we use it to infer f for new data g_j :

$$g_j \Rightarrow \boxed{\begin{array}{c} \text{Inference step} \\ \text{NN } (\hat{w}) \end{array}} \Rightarrow \hat{f}_{NNj}.$$

The hope is that \hat{f}_{NNj} is close to the (unknown) ground truth f_j , for example in terms of

$$\Delta = \|\hat{f}_{NNj} - f_j\|^2.$$

Beyond a point estimate, we would like to quantify the uncertainty of \hat{f}_{NNj} . The inference step with uncertainty quantification (UQ) can be summarized as

$$g_j \Rightarrow \boxed{\begin{array}{c} \text{Inference step} \\ \text{with UQ} \\ \text{NN } (\hat{w}) \end{array}} \Rightarrow \left\{ \begin{array}{c} \hat{f}_{NNj} \\ \hat{\Sigma}_{NNj} \end{array} \right\},$$

where $\hat{\mathbf{f}}_{NNj} = \mathbb{E}[\mathbf{f}_j|\mathbf{g}_j]$ is the posterior mean, and $\hat{\Sigma}_{NNj}$ its covariance. As $\mathbf{f} \in \mathbb{R}^N$ is high dimensional, $\hat{\Sigma}_{NNj} \in \mathbb{R}^{N \times N}$ is even larger, and in practice we often restrict attention to its diagonal (pixelwise variances). For imaging problems, one can thus visualize both a mean image and a variance (or standard deviation) image; examples will be provided in the Results section.

To go into more detail, we now discuss separately the supervised and unsupervised cases.

3.1. Supervised training data

We first consider the supervised case, where a labeled training dataset $\{\mathbf{g}_{Ti}, \mathbf{f}_{Ti}\}$ is available. The objective is to estimate the NN parameters $\hat{\mathbf{w}}$ using these paired data:

$$\text{Data } \{\mathbf{g}_{Ti}, \mathbf{f}_{Ti}\} \Rightarrow \boxed{\text{Supervised Training step}} \Rightarrow \hat{\mathbf{w}} .$$

$\text{NN}(\mathbf{w})$

Inside the supervised training block, the flow of variables can be illustrated as

$$\text{Data } \{\mathbf{g}_{Ti}, \mathbf{f}_{Ti}\} \Rightarrow \boxed{\text{NN}(\mathbf{w})} \Rightarrow \mathbf{f}_{NNi} \Rightarrow \boxed{\mathbf{H}} \Rightarrow \hat{\mathbf{g}}_{NNi} ,$$

where \mathbf{f}_{NNi} is the NN output corresponding to \mathbf{g}_{Ti} , and $\hat{\mathbf{g}}_{NNi} = \mathbf{H}\mathbf{f}_{NNi}$ is the corresponding prediction in the data space.

The main task is to define a criterion $J(\mathbf{w})$ to be minimized in order to obtain $\hat{\mathbf{w}}$. In classical NN training, the loss depends only on the discrepancy between NN output $\mathbf{f}_{NNi}(\mathbf{w})$ and reference \mathbf{f}_{Ti} :

$$J_{NN}(\mathbf{w}) = \sum_i \|\mathbf{f}_{Ti} - \mathbf{f}_{NNi}(\mathbf{w})\|^2, \quad (6)$$

which does not require the forward model \mathbf{H} .

In PINN methods, the criterion combines the output error and a physics-informed term:

$$J_{PI}(\mathbf{w}) = \sum_i \|\tilde{\mathbf{f}} - \mathbf{f}_{NNi}(\mathbf{w})\|^2 + \lambda \|\mathbf{g}_{Ti} - \mathbf{H}\mathbf{f}_{NNi}(\mathbf{w})\|^2, \quad (7)$$

where the first term can represent a data fidelity (or regularization) relative to some reference \bar{f} , and the second term enforces consistency with the forward model. One of the main goals of the proposed methodology is to show that such criteria (classical NN and physics-informed PINN) can be recovered as special cases of a more general Bayesian probabilistic formulation, which we detail next.

- **Step 1: probabilistic modeling of the training data.** We first focus on how the training data are generated. This step explicitly accounts for the forward model \mathbf{H} and the uncertainties in the data via a Bayesian approach. We assume that, given the true f_i and the forward model \mathbf{H} , the observed data $\{g_{Ti}\}$ are conditionally independent:

$$p(\{g_{Ti}\}|\{f_i\}) = \prod_i p(g_{Ti}|f_i), \quad (8)$$

with, for example, a Gaussian likelihood

$$p(g_{Ti}|f_i) = \mathcal{N}(g_{Ti} | \mathbf{H}f_i, v_{\epsilon i}\mathbf{I}). \quad (9)$$

Similarly, for the reference data $\{f_{Ti}\}$, we assume

$$p(\{f_{Ti}\}|\{f_i\}) = \prod_i p(f_{Ti}|f_i), \quad (10)$$

with

$$p(f_{Ti}|f_i) = \mathcal{N}(f_{Ti} | f_i, v_{f_i}\mathbf{I}). \quad (11)$$

Here, $v_{\epsilon i}$ and v_{f_i} are the variances governing the data generation process, encoding both the forward model physics and the measurement uncertainties. The process can be summarized schematically as

$$f_i \Rightarrow \boxed{\begin{array}{c} \text{Physics-based} \\ \text{Generating Data} \\ \text{System} \end{array}} \Rightarrow \begin{array}{l} f_{Ti} \sim p(f_{Ti}|f_i, v_{f_i}), \\ g_{Ti} \sim p(g_{Ti}|f_i, v_{\epsilon i}), \end{array}$$

where the notation $x \sim p(x)$ means that x is generated from the distribution $p(x)$.

We also assign a prior $p(f_i)$ to the true f_i , for example a Gaussian prior

$$p(f_i|\bar{f}, v_i) = \mathcal{N}(f_i | \bar{f}, v_i\mathbf{I}), \quad (12)$$

where \tilde{f} is a background (mean) image and v_i quantifies the variability of f_i around \tilde{f} .

- **Step 2: posterior of f_i given the training data.** Using Bayes' rule, the posterior distribution of f_i given the training data is

$$p(f_i | \{g_{Ti}, f_{Ti}\}) \propto p(g_{Ti} | f_i, v_{\epsilon i}) p(f_{Ti} | f_i, v_{f_i}) p(f_i | \tilde{f}, v_i). \quad (13)$$

With the Gaussian models in (9), (11), and (12), we can write

$$p(f_i | \{g_{Ti}, f_{Ti}\}) \propto \exp[-J(f_i)], \quad (14)$$

where

$$J(f_i) = \frac{1}{2v_{\epsilon i}} \|g_{Ti} - Hf_i\|^2 + \frac{1}{2v_{f_i}} \|f_{Ti} - f_i\|^2 + \frac{1}{2v_i} \|f_i - \tilde{f}\|^2. \quad (15)$$

It follows that the posterior is also Gaussian:

$$p(f_i | \{g_{Ti}, f_{Ti}\}) = \mathcal{N}(f_i | \hat{f}_i, \hat{\Sigma}_i), \quad (16)$$

with the usual linear-Gaussian expressions (here written schematically as)

$$\begin{cases} \hat{f}_i = [H^T H + \lambda_i I + \mu_i I]^{-1} (H^T g_{Ti} + \lambda_i f_{Ti} + \mu_i \tilde{f}), \\ \hat{\Sigma}_i = [H^T H + \lambda_i I + \mu_i I]^{-1} v_{\epsilon i}, \quad \lambda_i = \frac{v_{\epsilon i}}{v_{f_i}}, \quad \mu_i = \frac{v_{\epsilon i}}{v_i}. \end{cases} \quad (17)$$

These relations form the basic building blocks for the proposed BPINN formulation, both at training and inference stages.

- **Step 3: Bayesian modeling of the NN training.** We now consider the training step of the NN, denoting by $f_{NNi}(w)$ the NN output for input g_{Ti} and parameters w . The full flow of variables, from physics-based data generation through the NN and back to the data space, is

$$\boxed{\text{Generating Data System}} \Rightarrow \begin{Bmatrix} g_{Ti} \\ f_{Ti} \end{Bmatrix} \Rightarrow \boxed{\text{NN}(w)} \Rightarrow f_{NNi} \Rightarrow \boxed{H} \Rightarrow \hat{g}_{NNi}.$$

Focusing on the training step, where the goal is to estimate \mathbf{w} , we introduce the following probabilistic modeling:

$$\begin{cases} p(\mathbf{f}_{Ti}|\mathbf{w}) = \mathcal{N}(\mathbf{f}_{Ti} | \mathbf{f}_{NNi}(\mathbf{w}), v_{fi}\mathbf{I}), \\ p(\mathbf{g}_{Ti}|\mathbf{w}) = \mathcal{N}(\mathbf{g}_{Ti} | \mathbf{H}\mathbf{f}_{NNi}(\mathbf{w}), v_{\epsilon i}\mathbf{I}). \end{cases} \quad (18)$$

Using Bayes' rule with a prior $p(\mathbf{w})$, we obtain the posterior

$$p(\mathbf{w}|\{\mathbf{g}_{Ti}, \mathbf{f}_{Ti}\}) \propto \prod_i p(\mathbf{f}_{Ti}|\mathbf{w}) p(\mathbf{g}_{Ti}|\mathbf{w}) p(\mathbf{w}), \quad (19)$$

which can be rewritten as

$$p(\mathbf{w}|\{\mathbf{g}_{Ti}, \mathbf{f}_{Ti}\}) \propto \exp[-J(\mathbf{w})], \quad (20)$$

with

$$J(\mathbf{w}) = \sum_i \frac{1}{2v_{fi}} \|\mathbf{f}_{Ti} - \mathbf{f}_{NNi}(\mathbf{w})\|^2 + \frac{1}{2v_{\epsilon i}} \|\mathbf{g}_{Ti} - \mathbf{H}\mathbf{f}_{NNi}(\mathbf{w})\|^2 - \ln p(\mathbf{w}). \quad (21)$$

We can thus identify three components:

$$J_{NN}(\mathbf{w}) = \sum_i \frac{1}{2v_{fi}} \|\mathbf{f}_{Ti} - \mathbf{f}_{NNi}(\mathbf{w})\|^2, \quad (22)$$

$$J_{PI}(\mathbf{w}) = \sum_i \frac{1}{2v_{\epsilon i}} \|\mathbf{g}_{Ti} - \mathbf{H}\mathbf{f}_{NNi}(\mathbf{w})\|^2, \quad (23)$$

and the prior-induced term

$$J_{PR}(\mathbf{w}) = -\ln p(\mathbf{w}). \quad (24)$$

In other words, the classical NN loss J_{NN} , the physics-informed loss J_{PI} , and the regularization via the prior J_{PR} all arise from a single Bayesian posterior formulation.

The posterior $p(\mathbf{w}|\{\mathbf{g}_{Ti}, \mathbf{f}_{Ti}\})$ in (20)–(21) can be used to derive either point estimates of \mathbf{w} (e.g. MAP) or to quantify uncertainty in \mathbf{w} .

A useful choice for the prior $p(\boldsymbol{w})$ is a sparsity-enforcing prior [19], such as

$$p(\boldsymbol{w}) \propto \exp \left[-\gamma_w \|\boldsymbol{w}\|_\beta^\beta \right], \quad (25)$$

with $\beta \in (0, 2]$. The special case $\beta = 1$ (Laplace prior) is closely related to *dropout* techniques, which can be interpreted as a Monte Carlo approximation to Bayesian inference in NNs. In practice, computing the full posterior analytically is intractable, especially with nonlinear activation functions, and one typically resorts to approximate inference (e.g. variational methods or Monte Carlo dropout).

3.2. Unsupervised training data

In the unsupervised case, only the degraded training data $\{\boldsymbol{g}_{Ti}\}$ are available. Classical supervised NN methods cannot be applied, as there is no ground truth. This is precisely where the physics-informed PINN/BPINN framework is particularly valuable. The schematic data flow is

$$\text{Data } \{\boldsymbol{g}_{Ti}\} \Rightarrow \boxed{\text{NN}(\boldsymbol{w})} \Rightarrow \boldsymbol{f}_{NNi} \Rightarrow \boxed{\boldsymbol{H}} \Rightarrow \hat{\boldsymbol{g}}_{NNi}.$$

We can still follow the same Bayesian steps as in the supervised case, with appropriate modifications.

- **Data likelihood.** We assume that, given the true \boldsymbol{f}_i and the forward model \boldsymbol{H} , the data $\{\boldsymbol{g}_{Ti}\}$ are conditionally independent and Gaussian:

$$\begin{aligned} p(\{\boldsymbol{g}_{Ti}\}|\{\boldsymbol{f}_i\}) &= \prod_i \mathcal{N}(\boldsymbol{g}_{Ti} | \boldsymbol{H}\boldsymbol{f}_i, v_{\epsilon i} \boldsymbol{I}) \\ &\propto \exp \left[-\sum_i \frac{1}{2v_{\epsilon i}} \|\boldsymbol{g}_{Ti} - \boldsymbol{H}\boldsymbol{f}_i\|^2 \right]. \end{aligned} \quad (26)$$

- **Prior on \boldsymbol{f}_i .** We assign a prior $p(\boldsymbol{f}_i)$ to encode prior knowledge (e.g. smoothness or sparsity) about the unknowns. For imaging problems, a common choice is a Tikhonov, total variation, or generalized sparsity prior, for example

$$p(\boldsymbol{f}_i) \propto \exp \left[-\gamma \|\boldsymbol{D}\boldsymbol{f}_i\|_\beta^\beta \right], \quad (27)$$

where \boldsymbol{D} is a finite-difference (or other) operator, and $\beta \in (0, 2]$.

- **Posterior of f_i .** Using Bayes' rule, we obtain

$$p(f_i | \{g_{Ti}\}) \propto \exp[-J(f_i)], \quad (28)$$

with

$$J(f_i) = \sum_i \frac{1}{2v_{\epsilon i}} \|g_{Ti} - Hf_i\|^2 + \gamma \|Df_i\|_{\beta}^{\beta}. \quad (29)$$

- **Posterior over NN parameters w .** As in the supervised case, we can formulate a posterior over w by passing the data through the NN:

$$p(w | \{g_{Ti}\}) \propto \exp[-J(w)], \quad (30)$$

with

$$J(w) = \sum_i \frac{1}{2v_{\epsilon i}} \|g_{Ti} - Hf_{NNi}(w)\|^2 + \gamma_w \|w\|_{\beta_w}^{\beta_w}, \quad (31)$$

where the first term enforces physics-based consistency in the data space, and the second term imposes a prior (e.g. sparsity) on the NN weights. This posterior can then be used to estimate w and quantify uncertainty.

In both supervised and unsupervised regimes, the practitioner must still choose an appropriate NN architecture (depth, number of hidden units, type of convolutions, etc.) and optimization scheme (learning rate, batch size, stopping criteria, etc.). These choices make the practical implementation of BPINNs nontrivial and often require substantial experimentation. For a discussion on the choice of NN structures in inverse problems, we refer to [20, 21].

We summarize the two main steps of the proposed method (training) and (Inference and UQ), as they have been implemented, in Algorithm 1 and Algorithm 2. One main remark about the UQ, the whole computation of the posterior covariance is too costly and almost impossible. So, in Algorithm 2, only an approximate computation of the means and variances are implemented through simulated based Bayesian inference and the famous Drop-out technic often used in NNs implementation.

Algorithm 1 Bayesian Physics-Informed Neural Network for Inverse Problems (BPINN-IP) training steps.

Require: Forward operator H ;

- 1: Supervised data $\{g_{Ti}, f_{Ti}\}$ or unsupervised data $\{g_{Ti}\}$;
- 2: Noise variances $\{v_{\epsilon i}\}$, (optionally $\{v_{f_i}\}$ in supervised case);
- 3: Prior hyperparameters (γ_w, β_w) for $p(w)$; learning rate η ;
- 4: Maximum number of iterations K (or stopping criterion).
- 5: Initialize NN parameters $w^{(0)} \sim p(w)$

6: **for** $k = 0, 1, \dots, K - 1$ **do**

7: Sample a mini-batch $\mathcal{B} \subset \{1, \dots, N_T\}$ of training indices

8: **for** each $i \in \mathcal{B}$ **do**

9: **Forward pass in image space:** $f_{NNi} \leftarrow \text{NN}(g_{Ti}; w^{(k)})$

10: **Forward pass in data space (physics):** $\hat{g}_{NNi} \leftarrow H f_{NNi}$

11: **if** supervised **then**

12: Data-fidelity (NN) term:

$$J_{NN}^{(i)} \leftarrow \frac{1}{2v_{f_i}} \|f_{Ti} - f_{NNi}\|^2$$

13: **else**

14: $J_{NN}^{(i)} \leftarrow 0$ \triangleright no labeled f_{Ti} in unsupervised case

15: **end if**

16: Physics-informed term:

$$J_{PI}^{(i)} \leftarrow \frac{1}{2v_{\epsilon i}} \|g_{Ti} - \hat{g}_{NNi}\|^2$$

17: **end for**

18: Prior (regularization) term on NN parameters:

$$J_{PR}(w^{(k)}) \leftarrow -\ln p(w^{(k)}) \quad \text{e.g. } J_{PR}(w^{(k)}) = \gamma_w \|w^{(k)}\|_{\beta_w}^{\beta_w}$$

19: Total mini-batch loss:

$$J(w^{(k)}) \leftarrow \sum_{i \in \mathcal{B}} (J_{NN}^{(i)} + J_{PI}^{(i)}) + J_{PR}(w^{(k)})$$

20: Compute gradient $\nabla_w J(w^{(k)})$ by backpropagation

21: Update NN parameters (e.g. gradient descent, Adam):

$$w^{(k+1)} \leftarrow w^{(k)} - \eta \nabla_w J(w^{(k)})$$

22: **end for**

23: **Output:** trained parameters $\hat{w} = w^{(K)}$ approximating the posterior mode (MAP) of $p(w \mid \{g_{Ti}, f_{Ti}\})$

Algorithm 2 BPINN-IP inference and uncertainty quantification (UQ)

Require: Trained NN parameters \hat{w} (from Algorithm 1);

- 1: Forward operator H ;
- 2: New observed data g_j ;
- 3: Number of Monte Carlo samples T (e.g. $T = 20$ – 50).

4: **Initialization:**

Set $t \leftarrow 1$; initialize storage $\{f_{NNj}^{(t)}\}_{t=1}^T$ (and optionally $\{\hat{g}_{NNj}^{(t)}\}_{t=1}^T$).

5: **for** $t = 1, \dots, T$ **do**

6: Activate stochastic components of NN (e.g. dropout) using \hat{w}

7: **Forward pass in image space:**

$$f_{NNj}^{(t)} \leftarrow \text{NN}(g_j; \hat{w}, \text{stochastic})$$

8: **Optional forward pass in data space (physics check):**

$$\hat{g}_{NNj}^{(t)} \leftarrow H f_{NNj}^{(t)}$$

9: **end for**

10: **Posterior mean estimate (image space):**

$$\hat{f}_{NNj} \leftarrow \frac{1}{T} \sum_{t=1}^T f_{NNj}^{(t)}$$

11: **Posterior variance (pixelwise) estimate:**

$$\hat{\Sigma}_{NNj} \leftarrow \frac{1}{T-1} \sum_{t=1}^T (f_{NNj}^{(t)} - \hat{f}_{NNj}) \odot (f_{NNj}^{(t)} - \hat{f}_{NNj})$$

where \odot denotes elementwise (Hadamard) product.

12: **Optional data-space consistency check:**

$$\hat{g}_{NNj} \leftarrow \frac{1}{T} \sum_{t=1}^T \hat{g}_{NNj}^{(t)}, \quad \text{and compute } \|g_j - \hat{g}_{NNj}\|^2$$

as a physics-based quality indicator.

13: **Output:** posterior mean image \hat{f}_{NNj} and variance (or standard deviation) map $\hat{\Sigma}_{NNj}$, which can be visualized as an *expected value image* and an *uncertainty image*.

4. Application in infrared image processing

We consider two representative applications in infrared (IR) imaging: (i) infrared image restoration (deblurring), and (ii) infrared image super-resolution. Both are classical inverse problems in imaging science and computer vision [22, 23], and both can be written in the general form $\mathbf{g} = \mathbf{H}\mathbf{f} + \epsilon$ with appropriate modeling of the imaging physics.

4.1. Infrared image restoration

In this application, we consider a simplified but representative IR forward model:

$$g(x, y) = h(x, y) * \phi(f(x, y)) + \epsilon(x, y), \quad (32)$$

where $g(x, y)$ is the observed IR image, $h(x, y)$ is the point spread function (PSF) of the imaging system (accounting for heat diffusion in air and the optical response of the IR camera), $f(x, y)$ is the unknown surface temperature distribution, and $\epsilon(x, y)$ represents modeling and measurement errors.

The nonlinear pointwise mapping $\phi(\cdot)$ models the combined effects of: (1) surface emissivity, (2) ambient humidity and temperature, (3) background radiance, and (4) attenuation due to the distance between the surface and the sensor. More advanced emissivity–radiation models can be incorporated when available (see [24]).

Figure 1 illustrates these steps: nonlinear emissivity correction, diffusion–convolution, and final IR measurement.

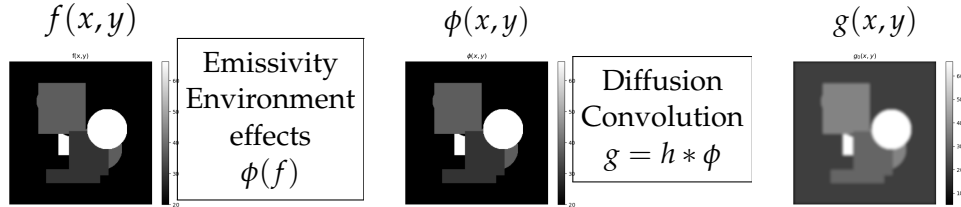


Figure 1: Infrared simplified forward model: from left to right. True temperature distribution $f(x, y)$; emissivity and environmental mapping $\phi(f)$; diffusion–convolution via the PSF h ; observed IR image g .

After discretization, the model becomes:

$$\mathbf{g} = \mathbf{H}\Phi\mathbf{f} + \epsilon, \quad (33)$$

where \mathbf{g} contains all IR image pixels, \mathbf{H} is the 2D convolution operator, Φ is a diagonal matrix representing the nonlinear emissivity mapping, and \mathbf{f} is the unknown temperature field. We again emphasize that only the operations $\mathbf{f} \mapsto \mathbf{H}\mathbf{f}$ and $\mathbf{g} \mapsto \mathbf{H}^T\mathbf{g}$ are needed in practical implementation of the optimization algorithms.

4.2. Infrared image super-resolution

In classical image super-resolution, the forward model is

$$\mathbf{g} = \mathbf{H}\mathbf{D}\mathbf{f} + \epsilon, \quad (34)$$

where \mathbf{f} is the high-resolution (HR) image, \mathbf{D} is the downsampling operator, \mathbf{H} accounts for optical filtering or sensor blur, and \mathbf{g} is the observed low-resolution (LR) image.

In the IR setting, we incorporate the same emissivity nonlinearity as in restoration:

$$\mathbf{g} = \mathbf{H}\mathbf{D}\Phi\mathbf{f} + \epsilon. \quad (35)$$

Thus, the super-resolution problem can be regarded as the same forward model as restoration, with an additional downsampling step before final measurement.

4.3. Implementation details

Because the forward models of restoration and super-resolution differ only by the presence of \mathbf{D} , their BPINN implementations follow nearly identical steps:

- **Generation of synthetic datasets.** We generate a training dataset $\{\mathbf{f}_{Ti}, \mathbf{g}_{Ti}\}$ using the forward model (33) or (35). This includes simulating emissivity variations, PSF convolution, downsampling (for SR), and controlled noise.
- **Neural network architecture.** We first validated all components of the BPINN on a simple fully connected NN with three hidden layers and ReLU activations. For realistic imaging, we used a U-Net architecture. More advanced architectures (unrolled networks, operator decompositions, plug-and-play variants, etc.) may also be employed depending on the task; see [20, 21] for discussion.

- **Loss functions and optimization.** Training follows the Bayesian framework developed in Section 4, combining

$$J(\boldsymbol{w}) = J_{NN}(\boldsymbol{w}) + J_{PI}(\boldsymbol{w}) + J_{PR}(\boldsymbol{w}),$$

with the supervised and unsupervised variants implemented exactly as described in Algorithms 1 and 2. We use gradient-based optimization (Adam) with tuned learning rates.

- **Performance monitoring.** During training, validation losses, PSNR, and SSIM are tracked across epochs.
- **Model saving and reuse.** The optimized parameters $\hat{\boldsymbol{w}}$ are saved and reloaded for inference and Monte Carlo dropout-based UQ.
- **Evaluation on simulated and real IR data.** Finally, trained models are tested on synthetic datasets and on real industrial IR images (with controlled emissivity and acquisition conditions).

A Python Jupyter notebook implementing all steps is available and will be publicly released upon acceptance of the paper.

Figures 2, 3, and 4 show representative examples of the synthetic training, validation, and test datasets.

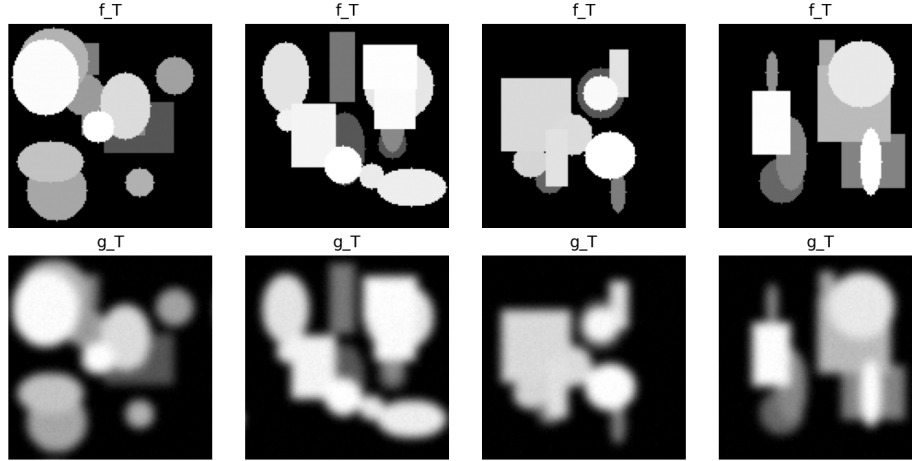


Figure 2: Examples of synthetic IR training data. Top: true temperature images f_{Ti} . Bottom: blurred and noisy observations g_{Ti} .

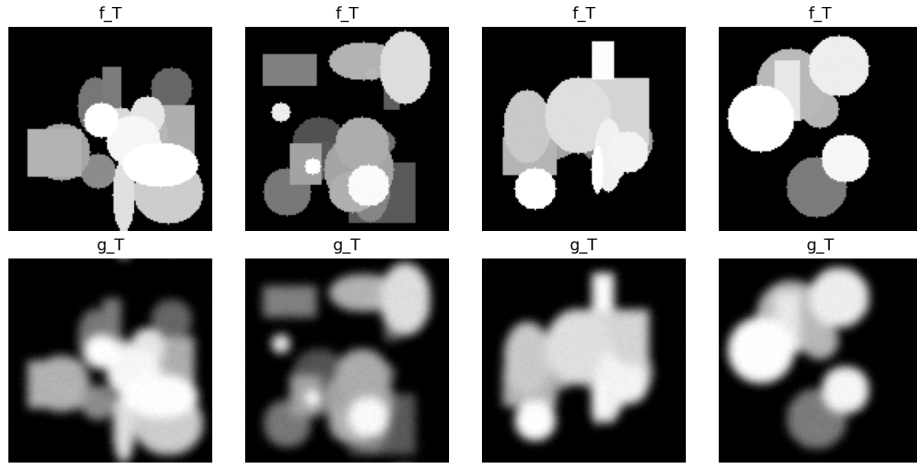


Figure 3: Examples of validation images used during training. Top: true images; Bottom: blurred and noisy observations.

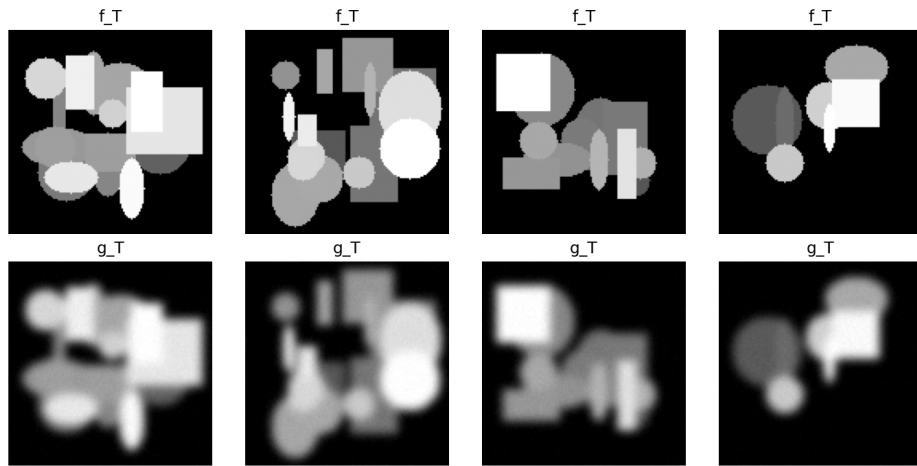


Figure 4: Examples of test images. Top: ground truth; Bottom: degraded inputs.

Figures 5, 6, and 7 show the evolution of the loss functions, PSNR, and SSIM during training for the NN, PINN, and BPINN, respectively.

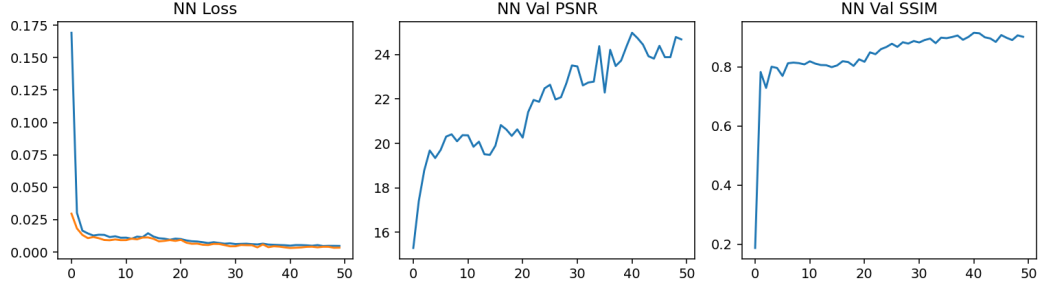


Figure 5: Training and validation losses, PSNR, and SSIM for the simple NN model.

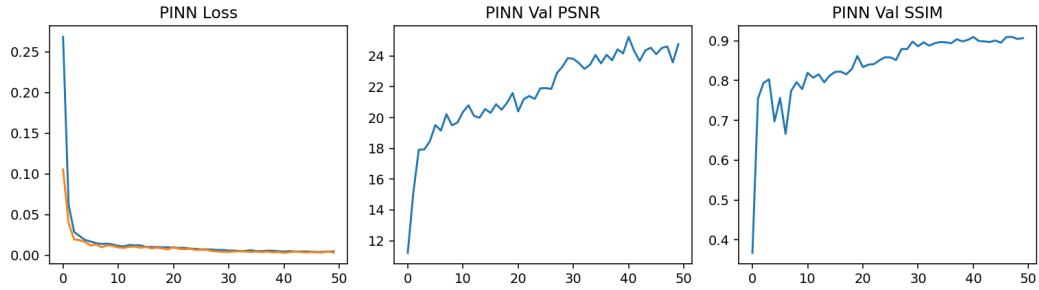


Figure 6: Training and validation losses, PSNR, and SSIM for the PINN model.

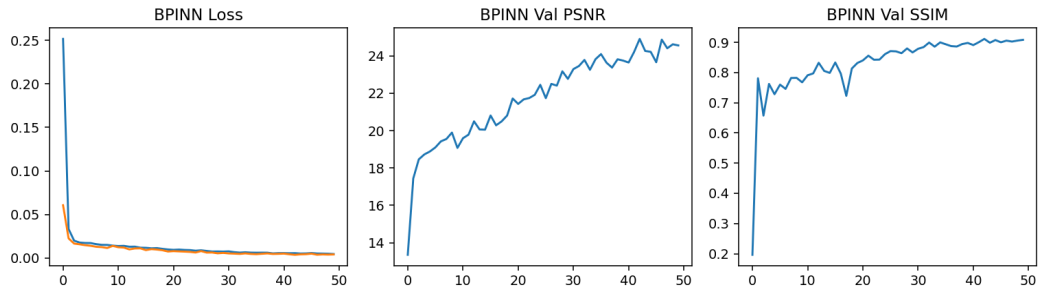


Figure 7: Training and validation losses, PSNR, and SSIM for the BPINN-IP model.

Figure 8 displays representative test results comparing NN, PINN, and BPINN-IP reconstructions for IR image restoration.

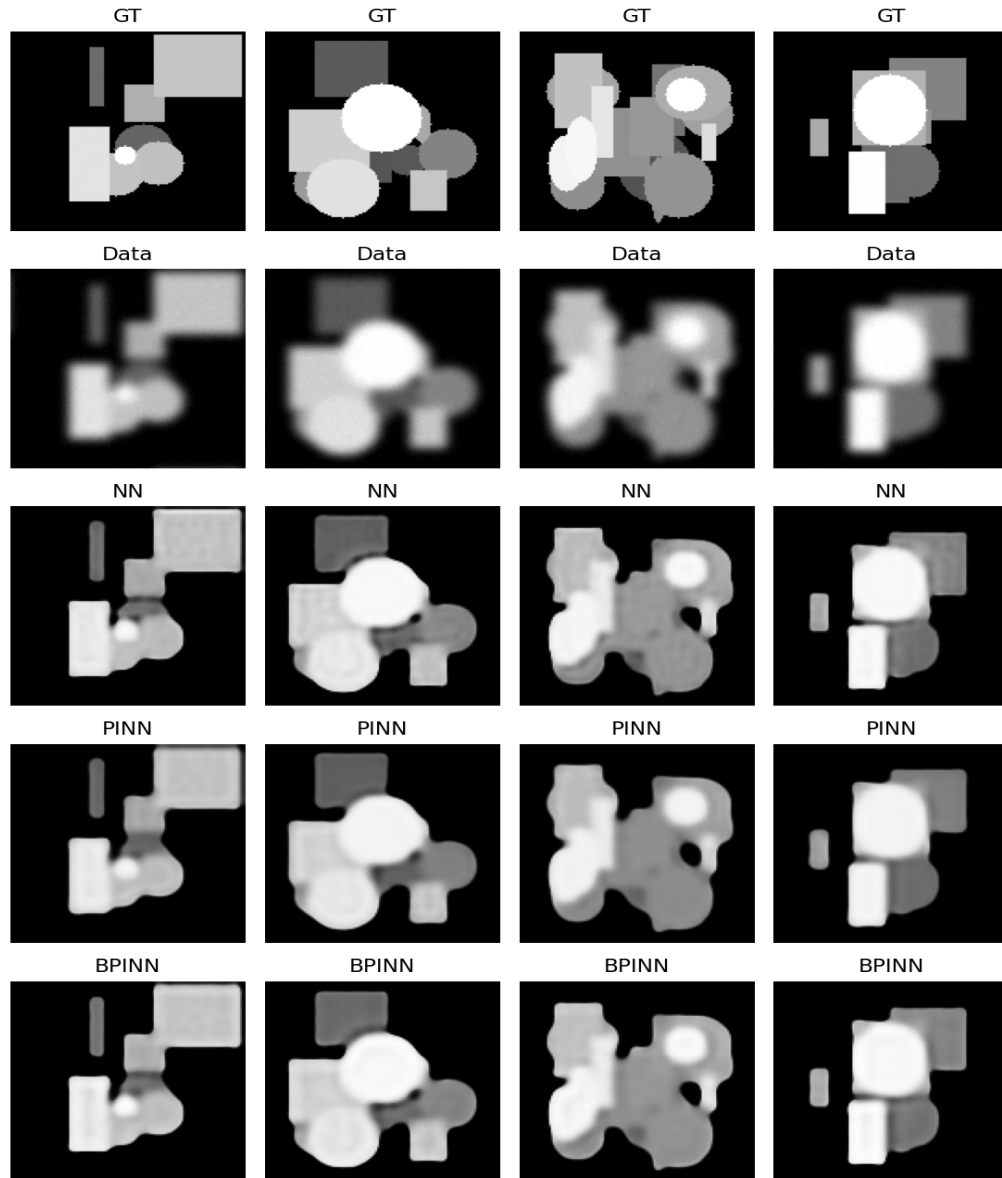


Figure 8: Test examples: ground truth, degraded input, and outputs of NN, PINN, and BPINN-IP models.

Figure 9 shows the posterior mean and variance images produced by the BPINN-IP using Monte Carlo dropout (Algorithm 2), illustrating uncertainty quantification.

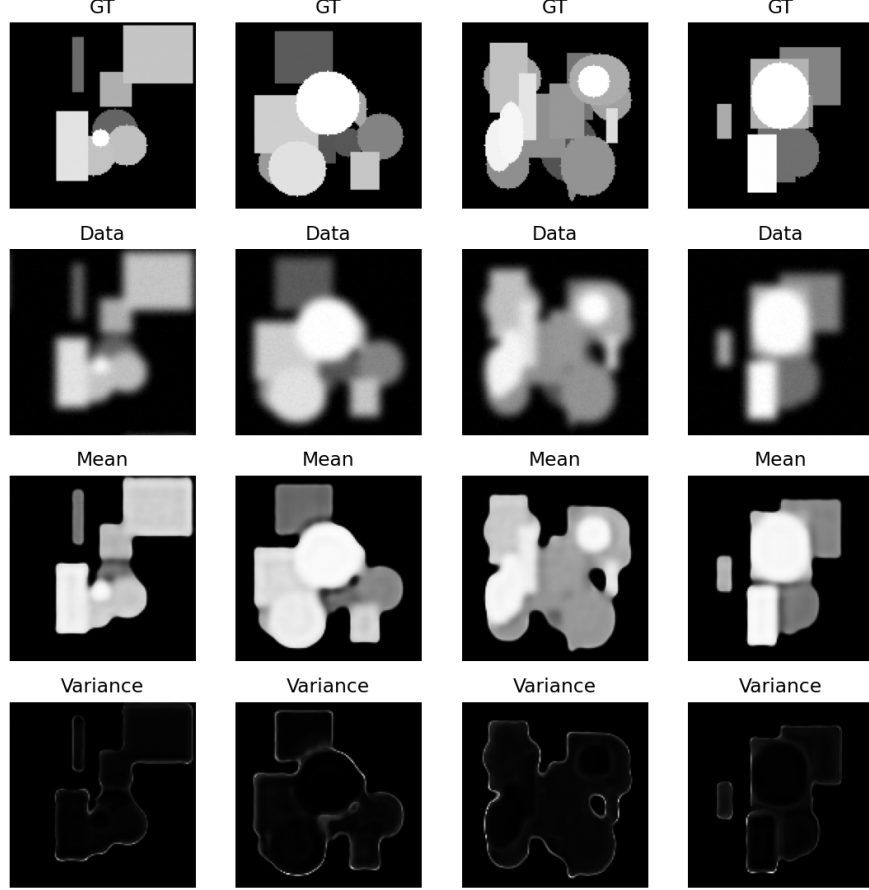


Figure 9: BPINN-IP inference results: posterior mean and variance images obtained via MC-dropout (approximate Bayesian Monte Carlo).

We used N_{train} synthetic images of size 128×128 for training, and N_{val} for validation and N_{test} for testing. We simulated two cases, one with great number of images (512, 128, 128) and one (128, 32, 32) respectively for N_{train} , N_{val} and N_{test} .

For both restoration and super-resolution, two neural network structures are used: one a CNN with a small number of layers, and the second

a more deeper based on UNET. Full implementation details, as well as the ablation experiments are provided in the supplementary material containing also the associated notebooks.

Figure 10 shows an example with a real infrared image which is degraded artificially and then restored using the three trained models NN, PINN, BPINN-IP.

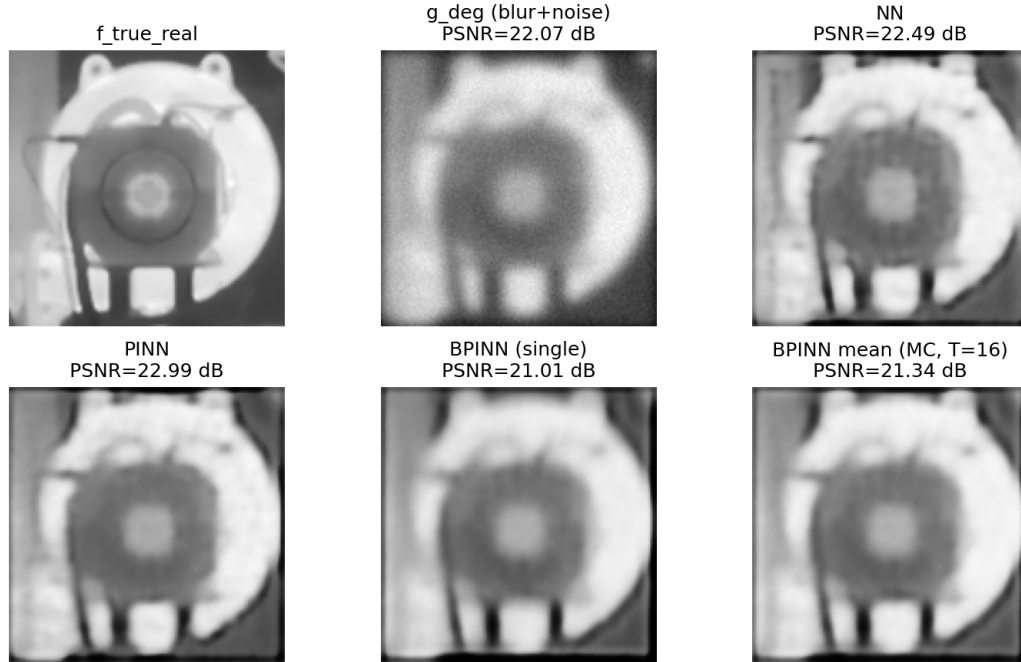


Figure 10: A real infrared image (top-left) is degraded (top-middle) and then restored using the three trained models NN, PINN, BPINN-IP single pass and the mean.

Figure 11 illustrates the results of the trained super-resolution networks NN, PINN, and BPINN-IP on a real IR image.

Many other examples are given in the supplementary document.

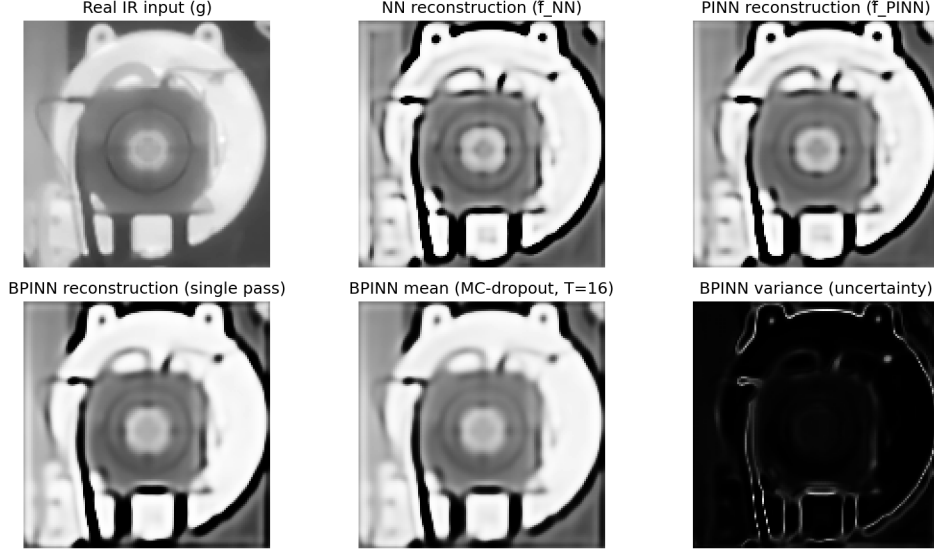


Figure 11: Results of the trained super-resolution networks NN, PINN, and BPINN-IP on a real IR image.

5. Discussion and Conclusion

This work introduced a new Bayesian formulation of Physics-Informed Neural Networks (BPINNs) for inverse problems (BPINN-IP) with specific application focus on infrared (IR) image restoration and super-resolution. The framework unifies classical regularization, Bayesian inference, and physics-informed deep learning into a single coherent probabilistic model.

From a methodological perspective, the key idea is to explicitly model the data-generation process using the forward operator H , possibly the nonlinear emissivity mapping Φ , and the associated measurement uncertainties. This generative viewpoint leads systematically to the Bayesian posterior distribution of the unknown image f and, simultaneously, to the posterior distribution of the neural network parameters w . Classical PINNs naturally emerge as the Maximum A Posteriori (MAP) solution of the BPINN-IP, while the full Bayesian model provides uncertainty quantification through posterior variances.

Several important observations can be drawn from the results:

- **Physical consistency improves reconstruction quality.**

Including the forward operator H in the training loss significantly stabilizes the inverse mapping, especially in the unsupervised setting where ground-truth images are unavailable.

- **The BPINN-IP posterior explains the role of loss terms.**
The decomposition

$$J(\boldsymbol{w}) = J_{NN}(\boldsymbol{w}) + J_{PI}(\boldsymbol{w}) + J_{PR}(\boldsymbol{w})$$

appears naturally from Bayes' theorem. The supervised term J_{NN} enforces consistency with labeled data, the physics-informed term J_{PI} enforces fidelity to the forward operator, and the prior term J_{PR} regularizes the NN parameters. This probabilistic interpretation provides a precise justification for the structure of PINN losses used in the literature.

- **Bayesian modeling provides principled uncertainty quantification.**
By interpreting dropout as an approximate Bayesian sampling method, BPINN-IPs provide pixelwise variance maps that identify regions of uncertainty.
- **BPINNs perform well on both synthetic and real IR data.**
The experiments confirm that the method is also robust to nonlinear emissivity effects, spatial blur induced by heat diffusion, and measurement noise. The use of a U-Net backbone further improves performance, showing that the BPINN-IP formulation can be combined with modern architectures.

Overall, the proposed BPINN-IP framework provides a general, interpretable, and computationally efficient methodology for solving inverse problems governed by physical models. It bridges the gap between classical Bayesian inference and physics-informed deep learning and offers a practical way to handle large-scale imaging problems where direct Bayesian computation is infeasible.

Future directions include:

1. extending the approach to nonlinear partial differential equations,
2. exploring more accurate emissivity–radiation models for IR thermography,

3. incorporating spatially varying PSFs and turbulence effects, and
4. applying BPINNs to multimodal fusion problems combining IR, visible, and depth measurements.

6. Conclusion

In this paper, we introduced a new point of view on the Bayesian Physics-Informed Neural Network (BPINN), specifically focusing on inverse problems (BPINN-IP). Even if the generic abbreviation BPINN has been used before for ODEs and PDEs, there was no sign of PINN and BPINN for the explicit inverse problems, where the forward model is a linear one, such as a convolution or super-resolution. Almost all the existing literature concerning PINN are for ODEs and PDEs. In this paper, we focussed on a more general integral linear inverse problems as in equation [1] or [32], and precisely for the discretized vector-matrix presentation as in equation [2] or [33].

By integrating Bayesian inference into the PINN structure, we achieved, not only more robust parameter estimation, but also meaningful uncertainty quantification, which is crucial for some real-world applications with noisy and incomplete data. Of course, the Bayesian approach has been used in different ways in NN based methods since many years. See for example [25, 26, 27, 28, 29, 30]. However, the proposed Bayesian approach in PINN is new, as we use a probabilist modeling in the generation or acquisition of the data set used for the training using the forward model and account for the errors. In fact the Physics is used both in the training data set generation, and in training of the NN. The obtained posterior probabilities can be used for the training part and for the testing or inference part.

For the application, our specific focus was on infrared image processing tasks like image deconvolution or super-resolution. Through the realistic simulation studies and a few real industrial examples, we demonstrated that BPINN-IP outperforms traditional methods in robustness and generalisation property of the trained NN, while reducing reliance on large labeled datasets. The ability to encode prior knowledge and physical constraints directly into the learning process significantly enhances generalization capabilities, especially in ill-posed and high-dimensional settings.

Future work will explore extending the BPINN framework to handle non-linear and dynamic inverse problems, optimizing network architectures for faster convergence, and validating the method on larger and more complex real-world data sets. With these improvements, we believe BPINN-IP can become a powerful, practical tool for solving a wide range of inverse problems across science and engineering.

Acknowledgments

References

- [1] S. Arridge, Optical tomography in medical imaging, *Inverse Problems* 15 (1999) R41–R93.
- [2] T. Bodin, M. Sambridge, Seismic tomography with the reversible jump algorithm, *Geophysical Journal International* 178 (2009) 1411–1436.
- [3] Y. Luo, L. Zeng, Z. He, A robust and efficient method for inverse problems with applications to structural health monitoring, *Mechanical Systems and Signal Processing* 45 (2014) 346–359.
- [4] K. Miya, Recent advancement of electromagnetic nondestructive inspection technology in japan, *IEEE Transactions on Magnetics* 38 (2002) 321–326.
- [5] K. H. Jin, M. T. McCann, E. Froustey, M. Unser, Deep convolutional neural network for inverse problems in imaging, *IEEE Transactions on Image Processing* 26 (2017) 4509–4522.
- [6] J. Ker, L. Wang, J. Rao, T. Lim, Deep learning applications in medical image analysis, *IEEE Access* 6 (2018) 9375–9389.
- [7] U. b. Waheed, T. Alkhalifah, E. Haghighat, C. Song, J. Virieux, Pinntomo: Seismic tomography using physics-informed neural networks, *Statistics and Computing* (2021).
- [8] V. Puzirev, Deep learning electromagnetic inversion with convolutional neural networks, *Geophysical Journal International* 218 (2019) 817–832.
- [9] H. Engl, M. Hanke, A. Neubauer, *Regularization of Inverse Problems, Mathematics and Its Applications*, Springer Netherlands, 1996.
- [10] J. T. Slagel, J. Chung, M. Chung, D. Kozak, L. Tenorio, Sampled tikhonov regularization for large linear inverse problems, *Inverse Problems* (2019) 24.

- [11] A. Mohammad-Djafari, Regularization, Bayesian inference and machine learning methods for inverse problems, *Entropy* 23 (12) (2021) 1673. [doi:10.3390/e23121673](https://doi.org/10.3390/e23121673).
- [12] L. Jiang, N. Ou, Multiscale model reduction method for bayesian inverse problems of subsurface flow, *Journal of Computational and Applied Mathematics* 319 (2017) 188–209.
- [13] M. Raissi, P. Perdikaris, G. Karniadakis, Physics-informed neural networks: A deep learning framework for solving forward and inverse problems involving nonlinear pdes, *Journal of Computational Physics* 378 (2019) 686–707.
- [14] L. Yang, X. Meng, G. E. Karniadakis, B-pinns: Bayesian physics-informed neural networks for forward and inverse pde problems with noisy data, *Journal of Computational Physics* 425 (2021) 109913.
- [15] E. Haghighat, M. Raissi, A. Moure, H. Gomez, R. Juanes, A physics-informed deep learning framework for inversion and surrogate modeling in solid mechanics, *Computer Methods in Applied Mechanics and Engineering* 379 (2021) 113741.
- [16] J. T. Slagel, J. Chung, M. Chung, D. Kozak, L. Tenorio, Sampled Tikhonov regularization for large linear inverse problems, *Inverse Problems* (2019) 24.
- [17] A. Beskos, A. Jasra, E. A. Muzaffer, A. M. Stuart, Sequential monte carlo methods for Bayesian elliptic inverse problems, *Statistics and Computing* 25 (2015) 727–737.
- [18] A. Fichtner, A. Zunino, L. Gebraad, Hamiltonian monte carlo solution of tomographic inverse problems, *Geophysical Journal International* 216 (2019) 1344–1363.
- [19] A. Mohammad-Djafari, Inverse problems in imaging science: From classical regularization methods to state of the art Bayesian methods, in: *International Image Processing, Applications and Systems Conference (IPAS)*, 2014, pp. 1–2. [doi:10.1109/IPAS.2014.7043317](https://doi.org/10.1109/IPAS.2014.7043317).

- [20] A. Mohammad-Djafari, N. Chu, L. Wang, L. Yu, Bayesian inference and deep learning for inverse problems, *Physical Sciences Forum* 9 (1) (2023).
- [21] A. Mohammad-Djafari, Interaction between model based signal and image processing, machine learning and artificial intelligence, *Proceedings* 33 (1) (2019).
- [22] H. Ayasso, A. Mohammad-djafari, Joint image restoration and segmentation using gauss-markov-potts prior models and variational Bayesian computation, in: 2009 16th IEEE International Conference on Image Processing (ICIP), 2009, pp. 1297–1300. [doi:10.1109/ICIP.2009.5413589](https://doi.org/10.1109/ICIP.2009.5413589).
- [23] F. Humblot, A. Mohammad-Djafari, Super-Resolution using Hidden Markov Model and Bayesian Detection Estimation Framework, *EURASIP Journal on Applied Signal Processing Special number on Super-Resolution Imaging: Analysis, Algorithms, and Applications* (2006) ID 36971, 16 pages.
- [24] A. Mohammad-Djafari, N. Chu, L. Wang, C. Cai, L. Yu, [Model based and physics informed deep learning neural network structures](#) (2024). [arXiv:2408.07104](https://arxiv.org/abs/2408.07104).
<https://arxiv.org/abs/2408.07104>
- [25] M. Seeger, Gaussian processes for machine learning, *International Journal of Neural Systems* 14 (02) (2004) 69–106. [doi:10.1142/S0129065704001899](https://doi.org/10.1142/S0129065704001899).
- [26] C. Blundell, J. Cornebise, K. Kavukcuoglu, D. Wierstra, Weight uncertainty in neural networks, in: *Proceedings of the 32nd International Conference on Machine Learning (ICML)*, Vol. 37 of *Proceedings of Machine Learning Research*, Lille, France, 2015, pp. 1613–1622. [arXiv:1505.05424](https://arxiv.org/abs/1505.05424).
- [27] A. Kendall, Y. Gal, What uncertainties do we need in Bayesian deep learning for computer vision?, in: *Advances in Neural Information Processing Systems (NeurIPS)*, Vol. 30, 2017, pp. 5574–5584. [arXiv:1703.04977](https://arxiv.org/abs/1703.04977).

- [28] S. Sun, G. Zhang, J. Shi, R. Grosse, [Functional variational Bayesian neural networks](#) (2019). [arXiv:1903.05779](#).
- [29] T. G. J. Rudner, Z. Chen, Y. W. Teh, Y. Gal, [Tractable function-space variational inference in Bayesian neural networks](#) (2023). [arXiv:2312.17199](#).
- [30] F. Wenzel, K. Roth, B. S. Veeling, J. Świątkowski, L. Tran, S. Mandt, J. Snoek, T. Salimans, R. Jenatton, S. Nowozin, How good is the Bayes posterior in deep neural networks really?, in: Proceedings of the 37th International Conference on Machine Learning (ICML), Vol. 119 of Proceedings of Machine Learning Research, PMLR, 2020, pp. 10248–10259. [arXiv:2002.02405](#).